Requirements for Gain/Oscillation in Yb^{3+}/Er^{3+}-Codoped Microring Resonators

Juan A. Vallés[a] and R. Gălătuş[b]
[a]Department of Applied Physics and I3A, University of Zaragoza, P. Cerbuna 12, 50009 Zaragoza, Spain; [b]Optoelectronics Group, Faculty of Electronics, Telecommunications and Information Technology, Technical University of Cluj-Napoca, Cluj-Napoca, Romania

ABSTRACT

A detailed model of the performance of a highly Yb^{3+}/Er^{3+}-codoped phosphate glass add-drop filter, which combines the propagation at resonance of both pump and signal powers inside the microring resonator with their interaction with the dopant ions, is used to analyze the requirements for gain/oscillation in these structures. Special attention is paid to the influence of additional coupling losses and asymmetry between the input/output couplers. It is concluded that, due to small signal gain saturation and the limited range of pump amplitude coupling coefficients, asymmetry does not greatly influence gain/oscillation requirements through the pump intensity build-up inside the ring. Asymmetry effect on small signal intensity transfer rate and threshold gain instead allows a significant lightening of the demanding doping ions concentrations requirements to achieve oscillation.

Keywords: Microring resonators, Yb^{3+}/Er^{3+}-codoped glass, gain/oscillation requirements, asymmetric structures.

1. INTRODUCTION

Microring resonators (MRR) have attracted much attention during the last decades as multifunctional components (filters[1], add-drop multiplexers[2], switches[4], modulators[4], etc.) in optical communication systems. Moreover, due to their fabrication scalability, functionalization and easiness in sensor interrogation MRRs with chip-integrated linear access waveguides they have recently emerged as promising candidates for scalable and multiplexable sensing platforms[5-8]. The near-infrared spectral range and, in particular, the 1.5-μm wavelength band (the gain band of the Er^{3+} ion) is already employed in several biological and chemical sensing tasks[9-11]. If gain is incorporated inside the ring, losses can be compensated, filtering and amplifying/oscillating functionalities are combined[12-13] and the sensing potentialities become enhanced[14]. But in return, modeling complexity of active structures greatly increases. In a preceding paper we developed a detailed model of the performance of a highly Yb^{3+}/Er^{3+}-codoped phosphate glass add-drop filter[15] which overcomes previous simpler models deficiencies[16]. This model assumes resonant behaviour inside the ring for both pump and signal powers and considers the coupled evolution of the rare-earth ions population densities and the optical powers that propagate inside the MRR. Since high dopant concentrations are needed to exploit the active potentialities of the structure phosphate glass with a high solubility for rare earth ions results an optimum host[17]. Moreover, energy-transfer inter-atomic processes become enhanced and have to be carefully considered in the numerical design. In this model the microscopic statistical formalism based on the statistical average of the excitation probability of the Er^{3+} ion in a microscopic level has been used to describe migration-assisted upconversion[18].

MRR-based passive components use mostly symmetrically coupled structures which maximize power in the drop port. However, asymmetric waveguide/resonator coupling may offer an optimum functional behavior[19], as in a critically-coupled MMR where the highest throughput attenuation (with subsequent optimization of the extinction ratio between the drop and through ports and crosstalk reduction between drop and add signals at the throughput port) is attainable[20] or when used as dispersion compensators in the time domain[21].

In this paper the model presented in Ref. 15 is used to determine the practical requirements to achieve amplification and oscillation in a highly Yb^{3+}/Er^{3+}-codoped phosphate glass MRR side-coupled to two straight waveguides for pump and signal input/output. In particular, the influence of additional coupling losses and the structure symmetry are fully discussed. In section 2 the active MRR model is briefly reviewed. In section 3 the characteristic parameters of the structure and the dependences on the circulating pump power of the amplitude gain coefficients for both pump and signal powers are presented. These coefficients describe the active behaviour of the device and allow the analysis of the

Optical Components and Materials XII, edited by Shibin Jiang, Michel J. F. Digonnet, Proc. of SPIE Vol. 9359, 93591R · © 2015 SPIE · CCC code: 0277-786X/15/$18 · doi: 10.1117/12.2078657

requirements for amplification and laser operation in both symmetric (in section 3) and asymmetric (in section 4) structures.

2. Yb^{3+}/Er^{3+}-CODOPED MICRORING RESONATOR MODEL

2.1 Active add-drop filter transfer functions.

The active structure under analysis is an MMR evanescently coupled to two straight parallel bus waveguides, commonly termed an add-drop filter. A scheme of this structure is shown in Fig. 1. Since we are interested in amplifiers and laser amplifiers the add port is not considered in the formalism. Single-mode single-polarization clockwise-direction propagation is considered and the MRR and bus waveguides are assumed to have the same complex mode amplitude propagation constant $\beta_c = \beta - j\alpha + jg$, where β is the phase propagation constant, α is the loss coefficient (due to scattering and bend) and g is the gain coefficient, which describes the evolution of the pump/signal mode amplitudes due to their interaction with the RE ions.

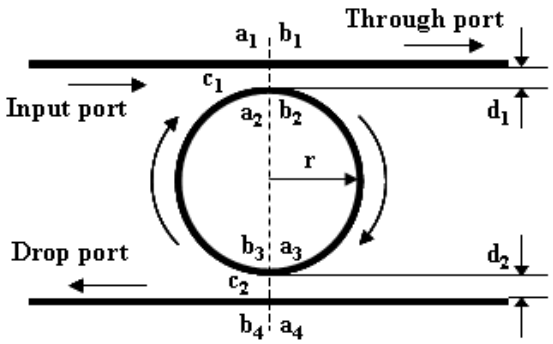

Figure 1. A microring resonator side-coupled to two parallel straight waveguides for pump and signal input/output. The scheme is not to scale.

In figure 1 r is the microring radius and $d_i\,(i=1,2)$ is the gap between the ring and the waveguides. Lossless intensity coupling and transmission coefficients at coupler $c_i\,(i=1,2)$ are $\mathrm{K}_i^0\,(i=1,2)$ and $T_i^0\,(i=1,2)$, satisfying $K_i^0 + T_i^0 = 1$. Correspondingly, $\kappa_i^0 = \left(\mathrm{K}_i^0\right)^{1/2}$ and $t_i^0 = \left(T_i^0\right)^{1/2}$ are the lossless amplitude coupling and transmission coefficients. Realistically, we also consider additional coupling losses at the waveguide/microring couplers. Even small additional coupling losses may have a large influence on the MRR performance[15]. Γ_i denotes the coefficient for additional intensity loss at the *ith* coupler. Therefore, the actual intensity coupling and transmission coefficients are $T_i = (1-\Gamma_i)\,T_i^0$, $K_i = (1-\Gamma_i)\,K_i^0$, which verify the relation $T_i + K_i = (1-\Gamma_i)$, whereas $t_i = T_i^{1/2}$ and $\kappa_i = K_i^{1/2}$ are the amplitude coupling and transmission coefficients, respectively. Mode confinement guarantees that interaction between the microring and bus waveguide cores is negligible outside the coupler regions.

If a_i and b_i are the input/output complex-field amplitudes at the couplers ports (*i=1,2* for the input/through ports at coupler I and *i=3,4* for the add/drop ports at coupler II) the exchange of optical power between the waveguides and the MMR can be described using the following scattering matrix relations:

$$\text{Coupler I: } \begin{vmatrix} b_1 \\ b_2 \end{vmatrix} = \begin{vmatrix} t_1 & -j\kappa_1 \\ -j\kappa_1 & t_1 \end{vmatrix} \begin{vmatrix} a_1 \\ a_2 \end{vmatrix} \quad ; \quad \text{coupler II: } \begin{vmatrix} b_3 \\ b_4 \end{vmatrix} = \begin{vmatrix} t_2 & -j\kappa_2 \\ -j\kappa_2 & t_2 \end{vmatrix} \begin{vmatrix} a_3 \\ a_4 \end{vmatrix} \tag{1}$$

The input/output transfer functions of the structure in figure 1, that is, the rates of the intensities from the input port to the output (through and drop) ports can be readily obtained:

$$I_{11} = \left|\frac{b_1}{a_1}\right|^2 = \frac{t_1^2 + (1-\Gamma_1)^2\, t_2^2\delta^2 - 2(1-\Gamma_1)\,t_1 t_2 \delta\cos(\beta L)}{1 + t_1^2 t_2^2 \delta^2 - 2t_1 t_2 \delta\cos(\beta L)},\; I_{41} = \left|\frac{b_4}{a_1}\right|^2 = \frac{\kappa_1^2\kappa_2^2\delta}{1 + t_1^2 t_2^2 \delta^2 - 2t_1 t_2 \delta\cos(\beta L)}, \tag{2}$$

where $L = 2\pi r$ is the length of the ring and $\delta = exp\left[\left(g-\alpha\right)L\right]$ is the round-trip gain.

2.2 Pump and signal powers evolution inside the active MRR.

We assume that the resonance condition ($\beta L = 2m\pi$, where m is an arbitrary integer) is fulfilled for both the pump and signal wavelengths and analyze the evolution of the pump and signal powers inside the MRR. On the one hand, the pump power that circulates inside the ring is best described using the intensity enhancement factor, *E*, the rate between the confined and the input pump intensities, which can be evaluated[15]:

$$E = \frac{\kappa_1^2\left\{1+t_2^2\delta\right\}}{\left(1-t_1t_2\delta\right)^2}\frac{\left\{1-\delta\right\}}{\left(\alpha-g\right)L} \tag{3}$$

On the other hand, for a resonant signal the transfer functions (Eq. (2)) become

$$I_{11} = \left\{\frac{t_1-\left(1-\Gamma_1\right)t_2\delta}{1-t_1t_2\delta}\right\}^2,\ I_{41} = \left\{\frac{\kappa_1\kappa_2}{1-t_1t_2\delta}\right\}^2\delta \tag{4}$$

Intensity rate to the through port, I_{11}, cancels when the critical coupling condition is verified:

$$t_1 = \left(1-\Gamma_1\right)t_2\delta\ . \tag{5}$$

This condition implies the complete destructive interference between the transmitted field and the internal field coupled into the output waveguide in c_1 so that the transmitted intensity drops to zero. From Eqs.(4) it can be deduced that if $g-\alpha > 0$ (i.e. $\delta > 1$), the device is a MRR amplifier and intensity rates in Eq. (4) may be greater than unity. When the denominator in Eqs. (4) cancels, that is, all the roundtrip losses are compensated by gain, I_{11} and I_{41} tend to infinity and the oscillation condition is reached. The threshold gain coefficient, g_{th}, can be calculated as:

$$g_{th} = \alpha_s - \frac{\ln\left[1-t_1t_2\right]}{2\pi r} \tag{6}$$

Finally, if $g > g_{th}$ the MRR behaves as a laser amplifier. Therefore, the fulfillment of the oscillation condition depends on the achievable signal gain coefficient, what forces a previous optimizing design based on the active MRR working conditions.

3. GAIN/OSCILLATION REQUIREMENTS FOR A SYMMETRIC STRUCTURE

3.1 The passive structure.

We have adopted for the calculations an air-cladded ridge guiding structure. This structure presents attractive features for sensing applications[22]. The passive parameters of the structure are summarized in table I.

Table I. Design parameters of the MRR structure

Parameter	***Value***
Waveguide cross section	1.5 μm x 1.5 μm
Substrate refractive index	1.51
Core refractive index	1.65
Pump wavelength	976 nm
Signal wavelength	1534 nm
Pump mode confinement factor	0.962
Signal mode confinement factor	0.757
Radius	15.40 μm
Pump resonant order	156
Signal resonant order	96
Propagation loss coefficient	0.25 dB/cm

At each coupler, the amplitude coupling ratios for pump and signal are functions of the central coupling gap, $d_i\,(i=1,2)$. They have been evaluated following Ref. 23 and are plotted in figure 2. The achievable range of values is quite limited, especially for the more confined pump power.

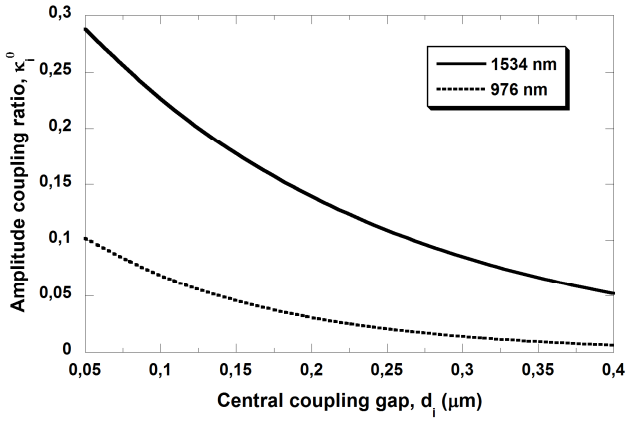

Figure 2. Amplitude coupling ratio for $\lambda = 1534\,nm$ (solid line) and $\lambda = 976\,nm$ (dotted line) as a function of the central coupling gap.

This range of coupling gap and accordingly of the amplitude coupling ratio is further limited when additional coupling losses are incorporated to the model. We estimate the range of additional coupling losses for our analysis from [24]. There the value 0.014 is reported for d=117±5 nm and it is concluded that these losses significantly increase when the gap width between the access waveguide and the microring is below this value.

3.2 Pump and small signal amplitude gain coefficients

Besides the lossless amplitude coupling coefficients and the additional pump coupling losses the pump intensity enhancement factor, E_p, and the intensity rate to the drop port, I_{41}, are basically determined by the pump and signal amplitude gain coefficients. They reflect the attenuation/increase induced on the pump/signal power by the stimulated transitions in the RE ions and, therefore, characterize the active contribution to the MRR performance. In order to calculate their dependence on the pump power that circulates inside the ring, we assume the model and spectroscopic parameters for an Yb/Er -codoped phosphate glass waveguide amplifier pumped in the 980-nm band in Ref. 25. It must be remarked that in our calculations the transversally-resolved microscopic statistical formalism of migration-assisted upconversion is used to accurately describe the contribution of energy-transfer mechanisms to the rate equations[25].

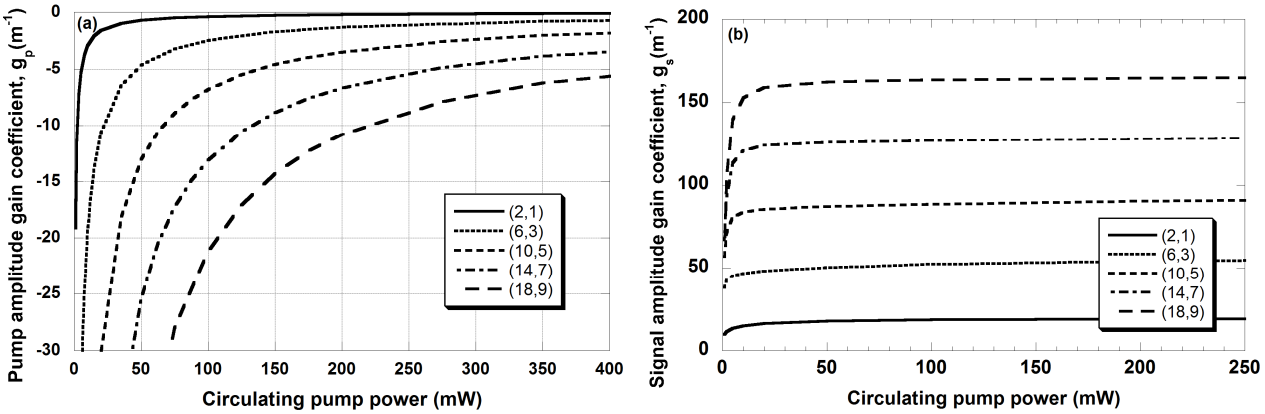

Figure 3. (a) Pump and (b) small signal amplitude gain coefficient in a lossless waveguide as a function of the average circulating pump power for 5 concentration pairs (n_{Yb}, n_{Er}). Units for the RE concentrations are 1 x 10^{26} ions/m^3

We have calculated the gain coefficients in a waveguide with L= 97.20 μm (2π x 15.47 μm) as a function of the average circulating pump power.These dependences are plotted in figure 3 for 5 concentration pairs (n_{Yb}, n_{Er}) where concentration units are 1 x 10^{26} ions/m^3. RE ions concentration pairs for the plot were chosen so that $n_{Yb}= 2n_{Er}$, since this concentration rate is often used experimentally. From now on we systematically use the subindex $\gamma = p, s$ for pump or signal, respectively, any time the labelled parameter is specific for the pump or the signal. From figure 3(a) it is clear that low pump powers are strongly attenuated as the dopant concentration increases whereas high pump powers are relatively less affected by rare earth absorption. On the other hand, g_s saturates for relatively low circulating pump power for any RE concentration pair. This performance is caused by the very short MRR length, which is much shorter than the waveguide amplifier optimal lengths for each circulating pump power and RE ions concentration pair.

3.3 Net gain requirements for a symmetric structure.

For simplicity we first analyze the requirements to achieve net gain and oscillation in a symmetric structure. Thus, in sections 3.3 and 3.4 we consider for both pump and signal powers equal lossless amplitude coupling ratios between the microring and the straight waveguides ($\kappa_\lambda^0 = \kappa_{1,\lambda}^0 = \kappa_{2,\lambda}^0$) and additional coupling losses ($\Gamma_\lambda = \Gamma_{1,\lambda} = \Gamma_{2,\lambda}$). We evaluate the net gain obtainable in the MRR amplifier as:

$$Net\ Gain\ (dB) = 10\log\left(I_{41}\right) \tag{7}$$

In Fig. 4 net gain is plotted as a function of the signal amplitude gain coefficient for three values of the lossless amplitude coupling coefficient and (a) $\Gamma_s = 0.005$ and (b) $\Gamma_s = 0.01$.

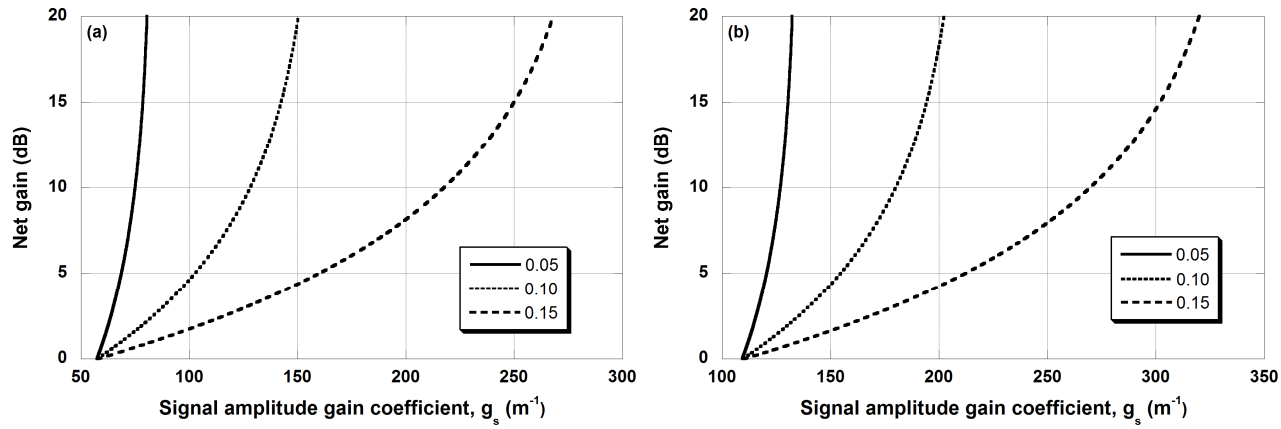

Figure 4. Net gain as a function of the signal gain coefficient for 3 values of the lossless amplitude coupling coefficient, κ_s^0, for (a) $\Gamma_s = 0.005$ y (b) $\Gamma_s = 0.01$.

As could be expected the value of g_s (and accordingly of the RE ion concentrations) necessary to achieve positive gain increases as the additional losses do. And, for instance, if $\Gamma_s = 0.01$, then $g_s > 100\,m^{-1}$ what implies $n_{Er} > 7x10^{26}\,m^{-3}$. Once positive net gain is achieved, it rate of growth is higher with lower κ_s^0.

3.4 Threshold gain and oscillation requirements for a symmetric structure.

Finally, in order to analyze the oscillation requirements, we have calculated the evolution of the threshold gain as a function of the lossless amplitude coupling coefficient, κ_s^0, for different values of the additional coupling losses. This evolution is plotted in figure 5. This figure illustrates the great influence on these requirements of Γ_s. If, for instance, $\kappa_s^0 = 0.05$, the threshold signal gain coefficient is 31.5 m^{-1}, 83.1 m^{-1}, 134.9 m^{-1} and 187.0 m^{-1} for Γ_s = 0, 0.005, 0.01, and 0.015, respectively. Hence, even small imperfections in the couplers fabrication could only be compensated by raising the RE doping level to achieve the necessary g_{th}. It has to be remarked that the unavoidable requirements of high

RE concentrations impose a host with a high solubility for RE ions, as phosphate glass where high dopant concentration can be achieved without serious ion clustering[17].

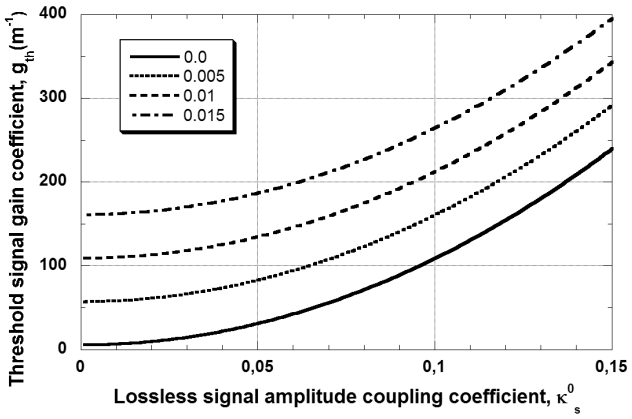

Figure 5. Threshold gain coefficient as a function of the lossless amplitude coupling coefficient, κ_s^0, for 4 different values of the additional coupling losses Γ_s

A further optimization could be accomplished if non symmetric structures are considered, allowing different values for the lossless amplitude coupling ratios and additional coupling losses between the microring and each straight waveguide.

4. GAIN/OSCILLATION REQUIREMENTS FOR AN ASYMMETRIC STRUCTURE

In order to parametrize the structure asymmetry, we use the relative variation of the lossless amplitude coupling coefficient, $\Delta\kappa_{r,\lambda}^0$, that is defined as $\Delta\kappa_{r,\lambda}^0 = \left(\kappa_{2,\lambda}^0 - \kappa_{1,\lambda}^0\right)/\kappa_{1,\lambda}^0$. As we limit the relative variations between -0.2 and 0.2 we assume the same additional coupling losses for both couplers. We'll also pay particular attention to the active critically-coupled structures and how their performance compares to the passive ones.

4.1 Asymmetry influence on pump enhancement.

In a symmetric structure for a given value of g_p, pump enhancement presents a maximum as a function of κ_p^0 for each Γ_p and this maximum shifts towards higher $\kappa_{1,p}^0$ values and rapidly decreases as additional losses increase[15].

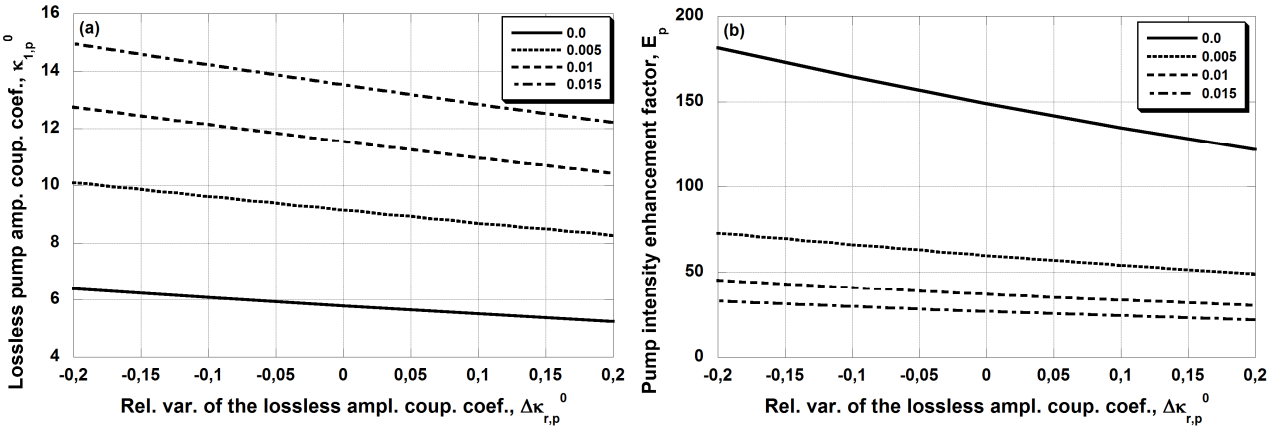

Figure 6. Evolution of the position and value of the pump enhancement maxima as a function of $\Delta\kappa_{r,p}^0$ for different values of $\Gamma_{1,s}$: (a) $\kappa_{1,p}^0$ and (b) E_p.

In Fig.6 the evolution of these maxima position and value are represented as a function of $\Delta\kappa_{r,p}^0$ for different values of $\Gamma_{1,s}$: (a) $\kappa_{1,p}^0$ and (b) E_p. Taking into account the range of values achievable for κ_p^0 in figure 2, it seems clear from figure 6 that $\Delta\kappa_{r,p}^0 > 0$ (maximum value shifts towards lower κ_p^0) favours pump enhancement. The saturation of small signal gain coefficient even for low circulation pump power in figure 3(b) attenuates the effect of the maximum value reduction.

4.2 Asymmetry influence on the drop/input port intensity rate, I_{14}.

Now we evaluate net gain for asymmetric MMR. In figure 7 the evolution with $\Delta\kappa_{r,s}^0$ of the dependence of net gain with g_s for $\kappa_{1,s}^0 = 0.1$ and $\Gamma_{1,s} = 0.005$. Although the minimum value of g_s does not change, the rate of growth is larger for $\Delta\kappa_{r,s}^0 < 0$.

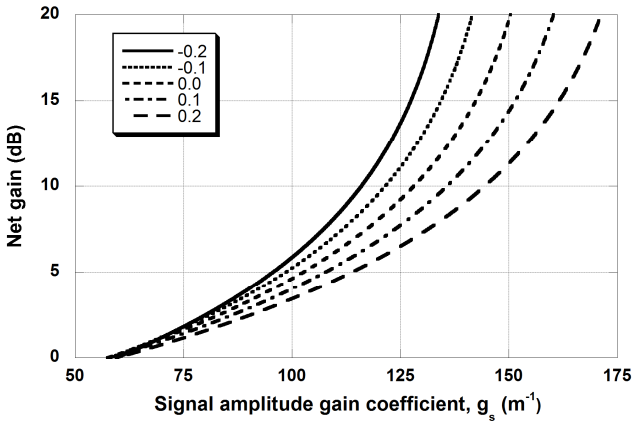

Figure 7. Evolution with $\Delta\kappa_{r,s}^0$ of the dependence of net gain with g_s for $\kappa_{1,s}^0 = 0.1$ and $\Gamma_{1,s} = 0.005$.

Besides, the performance in critical coupling conditions can be studied. However, in an active MRR for a given $\kappa_{1,s}^0$ the value of $\kappa_{2,s}^0$ that cancels the throughout intensity depends on the signal gain amplitude coefficient and on the additional losses.

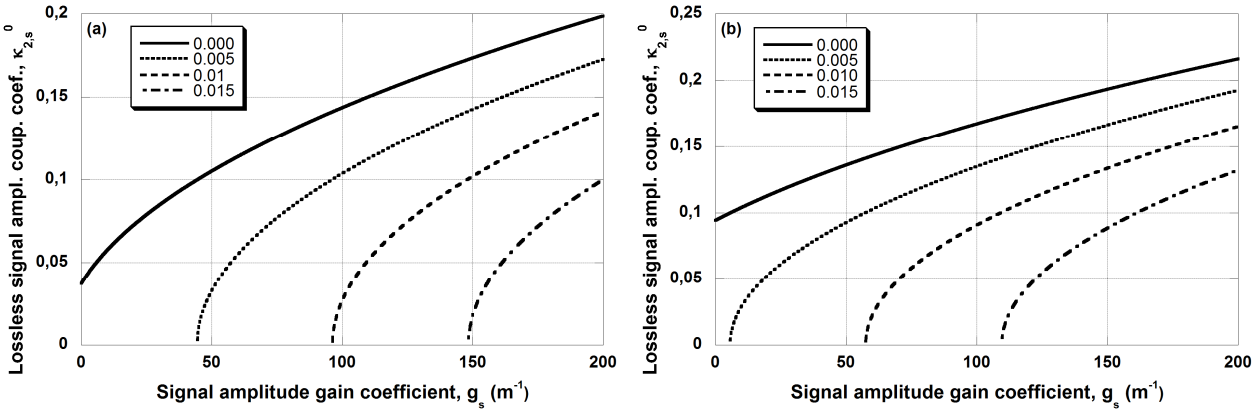

Figure 8. $\kappa_{2,s}^0$ for critical coupling as a function of g_s for 4 values of $\kappa_{1,s}^0$ and for (a) $\Gamma_{1,s} = 0.005$ and (b) $\Gamma_{1,s} = 0.01$.

In figure 8 the values of $\kappa_{2,s}^0$ for critical coupling are plotted as a function of g_s for 4 values of $\kappa_{1,s}^0$ and for (a) $\Gamma_{1,s} = 0.005$ and (b) $\Gamma_{1,s} = 0.01$. Differently from the passive performance output in the drop port is not maximized for

critical coupling. The net gain obtainable with the parameters in figure 7 is plotted in figure 8(a) and 8(b). Although, as we see in figure 6, higher net gain can be attained with other asymmetric configurations, in case the through contribution has to be minimized, significant net gain can still be achieved.

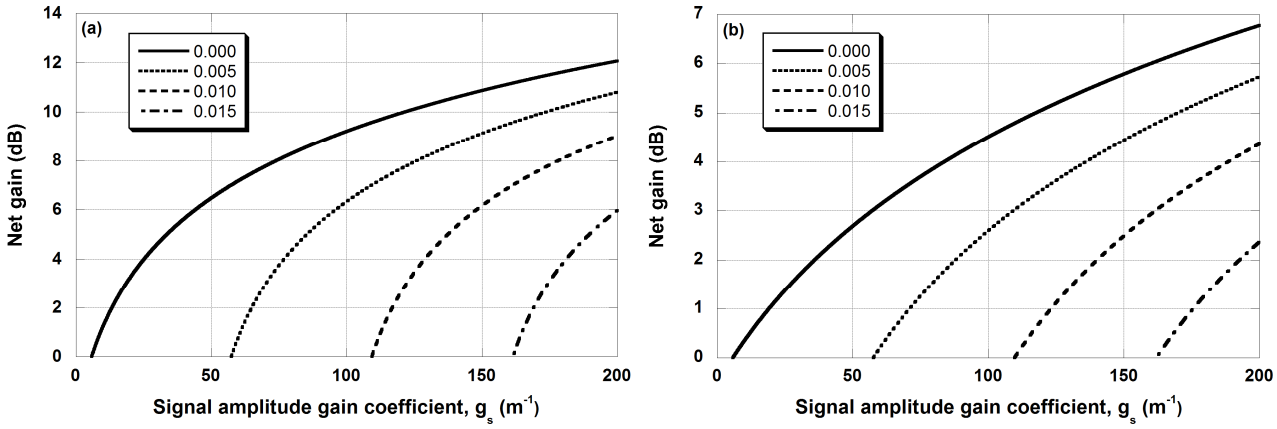

Figure 9. Net gain obtainable as a function of g_s for 4 values of $\kappa_{1,s}^0$ for the asymmetric critically-coupled configurations considered in figure 8 and for (a) $\Gamma_{1,s} = 0.005$ and (b) $\Gamma_{1,s} = 0.01$.

4.3 Asymmetry influence on threshold gain.

Finally we analyze the changes in threshold signal gain when asymmetric configurations are considered. In figure 10 the values of g_{th} are plotted as a function of $\Delta\kappa_{r,s}^0$ for different combinations of $\left(\kappa_{1,s}^0, \Gamma_{1,s}\right)$.

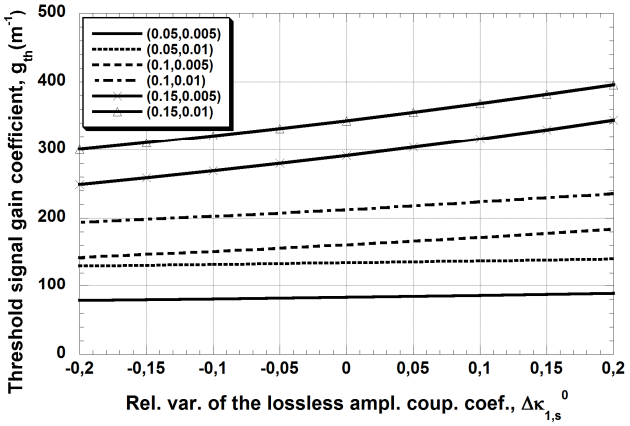

Figure 10. Variations in the threshold signal gain coefficient, g_{th}, as a function of $\Delta\kappa_{r,s}^0$ for different combinations of $\left(\kappa_{1,s}^0, \Gamma_{1,s}\right)$.

In figure 10 we can see how the necessary threshold gain value decreases for $\Delta\kappa_{r,s}^0 < 0$. This reduction is more significant for the higher additional coupling losses and contributes to relax the requirement for very high dopant concentrations.

5. CONCLUSIONS

An analysis of gain/oscillation requirements in a highly Yb^{3+}/Er^{3+}-codoped phosphate glass add-drop filter is carried out by using a detailed model that describes the evolution of resonant pump and signal powers inside the MRR structure while interacting with the RE ions. Special attention is paid to the influence of the additional coupling losses and the

structure symmetry. Much higher signal gain coefficients and threshold gain (and accordingly dopant concentrations) are required as the additional losses increase. This demand can be to some extent relieved by using asymmetric structures with an output coupler coupling coefficient lower than the input coupler one. Asymmetry has little influence on pump enhancement since due to the short length of the MRR signal gain saturation is achieved for relatively low circulating pump powers.

ACKNOWLEDGMENTS

This work was partially supported by the Spanish Ministry of Economy and Competitiveness under the TEC2013-46643-C2-2-R project, by the Diputación General de Aragón and by the project "Development and support of multidisciplinary postdoctoral programmes in major technical areas of national strategy of Research - Development - Innovation" 4D-POSTDOC, contract no. POSDRU/89/1.5/S/52603, project co-funded by the European Social Fund through Sectoral Operational Programme Human Resources Development 2007-2013.

REFERENCES

[1] Okamoto, H., Haraguchi, M. and Okamoto, T., "Filtering characteristic of a microring resonator with a gap," Electronics and Communications in Japan Part II-Electronics 89(5), 25-32 (2006).
[2] Little, B. E., Chu, S. T., Absil, P. P., Hryniewicz, J. V., Johnson, F.G., Seiferth, F., Gill, D., Van, V., King, O. and Trakalo, M., "Very high-order microring resonator filters for WDM applications," IEEE Phot. Technol. Lett. 16(10), 2263-2265 (2004).
[3] Först, M., Niehusmann, J., Plötzing, T., Bolten, J., Wahlbrink, T., Moormann, C., and Kurz, H., "High-speed all-optical switch in ion-implanted silicon-on-insulator microring resonators," Opt. Lett. 32(14), 2046-2048 (2007).
[4] M. Balakrishnan, M. Faccini, M. B. J. Diemeer, Klein, E. J., Sengo, G., Driessen, A., Verboom, W. and Reinhoudt, D. N., "Microring resonator based modulator made by direct photodefinition of an electro-optic polymer," Appl. Phys. Lett. 92(15), 153310 (2008).
[5] Ramachandran, A., Wang, S., Clarke, J., Ja, S., Goad, D., Wald, L., Flood, E., Knobbe, E., Hryniewicz, J., Chu, S., Gill, D., Chen, W., King, O. and Little, B., "A universal biosensing platform based on optical micro-ring resonators," Biosens. Bioelectron. 23, 939-944 (2008).
[6] Suter, J. D. and Fan, X., "Overview of the optofluidic ring resonator: a versatile platform for label-free biological and chemical sensing," In Engineering in Medicine and Biology Society. EMBC 2009. Annual International Conference of the IEEE, 1042-1044 (2009).
[7] Hunt, H. K. and Armani, A. M. "Label-free and chemical sensors," Nanoscale 2, 1544-1559 (2010).
[8] Baaske, M. and Vollmer, F., "Optical resonator biosensors: molecular diagnostic and nanoparticle detection on an integrated platform," ChemPhysChem 13(2), 427-436 (2012).
[9] Yang, G., White, I. M. and Fan, X., "An opto-fluidic ring resonator biosensor for the detection of organophosphorus pesticides," Sens. Actuators, B 133(1), 105-112 (2009).
[10] Sun, Y. and Fan, X., "Analysis of ring resonators for chemical vapor sensor development," Opt. Express 16(14), 10254-10268 (2008).
[11] Gohring, J. T., Dale, P. S. and Fan, X., "Detection of HER2 breast cancer biomarker using the opto-fluidic ring resonator biosensor," Sens. Actuators, B 146(1), 226-230 (2010).
[12] Amarnath, K., Grover, R., Kanakaraju, S. and Ho, P. T., "Electrically pumped InGaAsP-InP microring optical amplifiers and lasers with surface passivation," IEEE Photonics Technol. Lett. 17(11), 2280-2282 (2005).
[13] Hsiao, H.-K. and Winick, K. A., "Planar glass waveguide ring resonator with gain," Opt. Express 15(26), 17783-17797 (2007).
[14] He, L., Ozdemir, S. K., Zhu, J., Kim, W. and Zhang, L., "Detecting single viruses and nanoparticles using whispering gallery microlasers," Nat. nanotechnol. 6(7), 428-432 (2011).
[15] Vallés, J. A. and Galatus, R., "Modeling of Yb^{3+}/Er^{3+}-codoped microring resonators," Opt. Mater. (2014), http://dx.doi.org/10.1016/j.optmat.2014.10.028.
[16] Vallés, J. A. and Gălătuş, R., "Highly Yb^{3+}/Er^{3+}-Codoped Waveguide Microring Resonator Optimized Performance," IEEE Photon. Technol. Lett., 25(5), 457-459 (2013).

[17] Veasey, D. L., Funk, D. S., Peters, P. M., Sanford N. A., Obarski, G. E., Fontaine, N., Young, M., Peskin, A. P., Liu, W.-C., Houde-Walter, S. N.,Hayden, J. S.: "Yb/Er-codoped and Yb-doped waveguide lasers in phosphate glass," J. Non-Cryst. Solids 263&264, 369-381 (2000).
[18] Khoptyar, D., Sergeyev, S., Jaskorzynska, B., "Homogeneous upconversion in Er-doped fibres under steady state excitation. Analytical model and its Monte-Carlo verification," J. Opt. Soc. Am. B 22, 582-590 (2005).
[19] Vörckel, A., Mönster, M., Henschel, W., Bolivar, P. H., Kurz, H., "Asymmetrically coupled silicon-on-insulator microring resonators for compact add-drop-multiplexers," IEEE Photonics Technol. Lett. 15(7),921-923 (2003).
[20] Geuzebroek, D. H., Driessen, A. "Ring-resonator-based wavelength filters," in [Wavelength filters in fibre optics], pp. 341-379. Springer Berlin Heidelberg. (2006).
[21] Zhao, J. H., Madsen, C. K., [Optical Filter Design and Analysis] Wiley, NewYork, (1999).
[22] Passaro, V. M. N., Dell'Olio, F., De Leonardis, F., "Ammonia optical sensing by microring resonators," Sensors 7, 2741-2749 (2007).
[23] Ma, C. S., Yan, X., Xu, Y. Z., Qin, Z. K., Wang, X. Y., ," Characteristic analysis of bending coupling between two optical waveguides," Opt. Quantum Electron. 37, 1055-1067 (2005)
[24] Xia, F., Sekaric, L., Vlasov, Y. A., "Mode conversion losses in silicon-on-insulator photonic wire based racetrack resonators," Opt. Express 14, 3872-3886 (2006).
[25] Vallés, J. A., "Method for accurate gain calculation of a highly Yb^{3+}/Er^{3+}-codoped waveguide amplifier in migration-assisted upconversion regime," IEEE J. Quantum Electron., 47(8), 1151-1158 (2011).